Microwave Study of Superconductivity in Alkali-Metal-Doped C_{60} Films

S. H. Glarum,* S. J. Duclos, and R. C. Haddon*

Contribution from AT&T Bell Laboratories, Murray Hill, New Jersey 07974-2070.
Received October 10, 1991

Abstract: We have studied the doping of films of C_{60} and C_{70} by low-temperature alkali-metal vaporization. These films develop visible phase boundaries during the doping process. By using Raman, ESR, and microwave loss (superconductivity) spectroscopies to characterize the doped films in situ, we have established the compositions which occur under these conditions. We report the first preparation of a K_3C_{60} film in which the superconducting transition temperature approaches that of the bulk materials (T_c = 19 K) and the first observation of superconductivity in an Rb_3C_{60} film (T_c = 25 K). With C_{60} films, all of the alkali metals studied (A = Na, K, Rb, Cs) eventually form the insulating A_6C_{60} phase after prolonged doping. The A_3C_{60} phase occurs for A = Na, K, and Rb, but only the K and Rb compounds superconduct above 4 K. Large frequency shifts accompanying the superconducting transition indicate macroscopic microwave flux exclusion volumes and set critical field limits. In low magnetic fields, superconductivity is dominated by weak link behavior, resembling that of polycrystalline high-T_c materials. Superconductivity was not observed with alkali-metal-doped C_{70} films.

The identification of the fullerenes[1] and their subsequent synthesis[2] have stimulated interest in the properties of these new materials. In a series of papers we demonstrated that C_{60} and C_{70} could be doped with alkali metals to become conductive and that K_xC_{60} and Rb_xC_{60} are superconductors.[3-5] In our initial study we showed that there was a maximum conductivity for each alkali metal/fullerene combination beyond which further doping reduced the conductivity.[3]

Recent work has confirmed our hypotheses[3,4] for the stoichiometry and structure of the superconducting phase. The superconducting composition is A_3C_{60} (A = K, Rb),[6] and the structure is FCC,[7] with the alkali-metal ions occupying the tetrahedral and octahedral interstitial sites in the C_{60} lattice. This composition has also been identified as the metallic phase.[8-10] At higher doping levels the insulating A_6C_{60} composition[3] is obtained, and this is now known to possess a BCC structure.[11] New compositions have been reported, with substantially increased superconducting transition temperatures,[12-14] and a BCT A_4C_{60} structure has been identified.[15]

^{13}C NMR spectroscopy shows that only the C_{60} and K_3C_{60} phases are stable in K_xC_{60} for $x \leq 3$.[16] Recent photoemission studies[17] conclude that the data for potassium doping are best accounted for in terms of the presence of only three phases, C_{60}, K_3C_{60}, and K_6C_{60}. Superconducting K_3C_{60} shows a very large decrease in T_c with increasing pressure.[18,19] In a study on a series of FCC A_3C_{60} superconductors it was shown that T_c increases with the lattice constant and, by implication, with the density of states at the Fermi level.[5,20] Magnetization studies of superconductivity in powders have confirmed type II behavior and reported critical fields, $H_{c1}(0) \sim 130$ G and $H_{c2}(0) \sim 5 \times 10^5$ G, as well as hysteretic behavior due to flux pinning.[21]

Although the observation of superconductivity in alkali-metal C_{60} compounds has attracted considerable attention to these materials, our present knowledge of their intrinsic physical and chemical properties is still fragmentary. Because of extreme sensitivity to oxygen, most studies have been restricted to powdered samples prepared and maintained in sealed tubes and it has been difficult to carry out more than one type of experiment on any specific sample.

The transport properties of thin films of alkali-metal-doped C_{60} are among the most interesting features of these materials. While resistive measurements have shown that the films can be metallic,[3,10] comparatively little has yet been published about their properties. The only observation of superconductivity in a doped C_{60} film came in the original report on K_xC_{60},[4] in which zero resistance was not achieved until 5 K. There is no guarantee that the doping of thin films and bulk powders should be identical, and the films offer a visual advantage for observing the changes taking place during doping. The films we discuss have the further advantage of being examinable by multiple techniques, ESR, Raman,

(1) Kroto, H. W.; Heath, J. R.; O'Brien, S. C.; Curl, R. F.; Smalley, R. E. *Nature* **1985**, *318*, 162-164.
(2) Kratschmer, W.; Lamb, L. D.; Fostiropoulos, K.; Huffman, D. R. *Nature* **1990**, *347*, 354-358.
(3) Haddon, R. C.; Hebard, A. F.; Rosseinsky, M. J.; Murphy, D. W.; Duclos, S. J.; Lyons, K. B.; Miller, B.; Rosamilia, J. M.; Fleming, R. M.; Kortan, A. R.; Glarum, S. H.; Makhija, A. V.; Muller, A. J.; Eick, R. H.; Zahurak, S. M.; Tycko, R.; Dabbagh, G.; Thiel, F. A. *Nature* **1991**, *350*, 320-322.
(4) Hebard, A. F.; Rosseinsky, M. J.; Haddon, R. C.; Murphy, D. W.; Glarum, S. H.; Palstra, T. T. M.; Ramirez, A. P.; Kortan, A. R. *Nature* **1991**, *350*, 600-601.
(5) Rosseinsky, M. J.; Ramirez, A. P.; Glarum, S. H.; Murphy, D. W.; Haddon, R. C.; Hebard, A. F.; Palstra, T. T. M.; Kortan, A. R.; Zahurak, S. M.; Makhija, A. V. *Phys. Rev. Lett.* **1991**, *66*, 2830-2832.
(6) Holczer, K.; Klein, O.; Huang, S.-M.; Kaner, R. B.; Fu, K.-J.; Whetten, R. L.; Diederich, F. *Science* **1991**, *252*, 1154-1157.
(7) Stephens, P. W.; Mihaly, L.; Lee, P. L.; Whetten, R. L.; Huang, S.-M.; Kaner, R.; Diederich, F.; Holczer, K. *Nature* **1991**, *351*, 632-634.
(8) Benning, P. J.; Martins, J. L.; Weaver, J. H.; Chibante, L. P. F.; Smalley, R. E. *Science* **1991**, *252*, 1417-1418.
(9) Wertheim, G. K.; Rowe, J. E.; Buchanan, D. N. E.; Chaban, E. E.; Hebard, A. F.; Kortan, A. R.; Makhija, A. V.; Haddon, R. C. *Science* **1991**, *252*, 1419-1421.
(10) Kochanski, G. P.; Hebard, A. F.; Haddon, R. C.; Fiory, A. T. *Science*, submitted for publication.
(11) Zhou, O.; Fischer, J. E.; Coustel, N.; Kycia, S.; Zhu, Q.; McGhie, A. R.; Romanow, W. J.; McCauley Jr., J. P.; Smith, A. B., III; Cox, D. E. *Nature* **1991**, *351*, 462-464.
(12) Kelty, S. P.; Chen, C.-C.; Lieber, C. M. *Nature* **1991**, *352*, 223-224.
(13) Tanigaki, K.; Ebbesen, T. W.; Saito, S.; Mizuki, J.; Tsai, J. S.; Kubo, Y.; Kuroshima, S. *Nature* **1991**, *352*, 222-223.
(14) Iqbal, Z.; Baughmann, R. H.; Ramakrishna, B. L.; Khare, S.; Murthy, N. S.; Bornemann, H. J.; Morris, D. E. *Science* **1991**, *254*, 826-829.
(15) Fleming, R. M.; Rosseinsky, M. J.; Ramirez, A. P.; Murphy, D. W.; Tully, J. C.; Haddon, R. C.; Siegrist, T.; Tycko, R.; Glarum, S. H.; Marsh, P.; Dabbagh, G.; Zahurak, S. M.; Makhija, A. V.; Hampton, C. *Nature* **1991**, *352*, 701-703.
(16) Tycko, R.; Dabbagh, G.; Rosseinsky, M. J.; Murphy, D. W.; Fleming, R. M.; Ramirez, A. P.; Tully, J. C. *Science* **1991**, *253*, 884-886.
(17) Chen, C. T.; Tjeng, L. H.; Rudolf, P.; Meigs, G.; Rowe, J. E.; Chen, J.; McCauley Jr., J. P.; Smith, A. B., III; McGhie, A. R.; Romanow, W. J.; Plummer, E. W. *Nature* **1991**, *352*, 603-605.
(18) Schirber, J. E.; Overmyer, D. L.; Wang, H. H.; Williams, J. M.; Carlson, K. D.; Kini, A. M.; Pellin, M. J.; Welp, U.; Kwok, W.-K. *Phys. C* **1991**, *178*, 137-139.
(19) Sparn, G.; Thompson, J. D.; Huang, S.-M.; Kaner, R. B.; Diederich, F.; Whetten, R. L.; Gruner, G.; Holczer, K. *Science* **1991**, *252*, 1829-1831.
(20) Fleming, R. M.; Ramirez, A. P.; Rosseinsky, M. J.; Murphy, D. W.; Haddon, R. C.; Zahurak, S. M.; Makhija, A. V. *Nature* **1991**, *352*, 787-788.
(21) Holczer, K.; Klein, O.; Gruner, G.; Thompson, J. D.; Diederich, F.; Whetten, R. L. *Phys. Rev. Lett.* **1991**, *67*, 271-274.

0002-7863/92/1514-1996$03.00/0

and microwave loss, eliminating the uncertainties arising in the comparison of different experiments with different samples.

Experimental Section

Sample Preparation. The fullerenes were isolated by chromatography[3] of soot extract.[2] The C_{60} was taken up in CS_2 and reprecipitated in hexane which was agitated with a slow stream of nitrogen. C_{60} was collected on a fine filter paper and dried at the pump after which the material could be isolated as a mustard crust which separated easily from the filter paper. The reprecipitation procedure ensured that the C_{60} samples were free from oils and organic contaminants.

All experiments were performed in sealed Suprasil ESR tubes of 2-mm internal diameter. Alkali metals were introduced into the sample tubes in a drybox in glass capillaries after the fullerene was present as a powder[4] or a film. Tubes were then sealed under vacuum without exposing their contents to the atmosphere.

Films were grown by attaching the tube to a vacuum line and subliming the C_{60} or C_{70} with a 1-cm-long nichrome coil of No. 30 wire wrapped around the tube's bottom. The heating voltage was chosen so that a visible sublimation deposit appeared just above the coil after 30 s. A thermocouple in a similar, open tube indicated an internal temperature of 425 °C. After 5 min, the sublimation deposit had grown to a visible length of 2 cm, with colors ranging from dark brown through amber to yellow (C_{60}). The deposit was of varying thickness, up to five interference fringes being apparent when viewed under monochromatic illumination (5461 Å). The sample was transferred under vacuum to a He-filled drybox and an alkali-metal-filled capillary containing ~50 mg metal inserted. The tube was then returned to the vacuum line, evacuated, and sealed.

Film Doping. The film was doped by placing the tube in an oven at a temperature for which the metal's vapor pressure was about 10^{-4} Torr. Representative doping temperatures were 180 °C for Na, 130 °C for K, 100 °C for Rb, and 60 °C for Cs. Doping was monitored by color changes in the C_{60} film. After 30 min, a magenta band appeared at the thin end of the film, closest to the metal source, being visible in regions of the film too thin to be seen directly before doping. On continued doping, this band advanced, typically 2–3 mm over 15 min, into the thicker portion of the film with a second very dark band developing just ahead of it. After several hours of doping, the central band had grown to a width of 1 mm, with sharp boundaries separating it from the magenta region above (closest to the metal source) and the thicker film below. The film was monitored during doping by Raman, ESR, and microwave loss (superconductivity)[22-24] spectroscopies. By varying the position of the sample in the microwave cavity, it was established that the maximum superconducting response occurred with the central band in the center of the cavity. The strongest responses were found with the central band about 1 mm wide in a portion of the film ~0.5 μm thick, based on interference fringe observations. Prolonged doping reduced this response 100-fold, although traces of superconductivity could still be detected near the lower edge where the film was estimated to be several microns thick.

After doping had reached an optimal level, it was found that the superconducting response could be significantly enhanced by annealing at 200 °C. This was done using a second heating coil, 2 cm long, positioned on the film. No additional doping occurs with the alkali-metal source at room temperature, and annealing should principally influence the crystallinity and dopant distribution within the thickness of the film.

Instrumentation. The microwave bridge used in these experiments is of conventional homodyne design, using a voltage-tunable Gunn diode source (M/A-COM MA87840) and a Varian V-4531 X-band cavity with an LTR-3 liquid He Dewar assembly (APD Cryogenics). A PAR 5210 lock-in amplifier served as modulation source and signal detector, and a PAR 5209 was used for automatic frequency control. This instrumentation was interfaced to a PC for data acquisition and analysis. The magnetic field was controlled by a Varian V-FR2503 field-dial unit modified for sweeping by a computer-generated ramp. Field calibrations were made with either a tracking NMR fluxmeter or a DTM-141D Teslameter (GMW Associates) and frequency measurements with an HP-5350B counter.

Raman spectra were obtained using approximately 15 mW of the 514.5-nm Ar ion laser line on a 100 μm × 300 μm spot in a back-scattering geometry. A scanning Spex double monochromator and conventional photon counting were used to collect the spectra. Scanning speeds of 10 cm^{-1}/min were used, and all spectra have been acquired at room temperature.

Table I. Raman A_g Mode in Alkali-Metal-Doped C_{60}

dopant	Raman shift (cm^{-1})	inferred stoichiometry
none	1458	C_{60}
Na	1449	Na_3C_{60}
	1433	Na_6C_{60}
K	1446	K_3C_{60}
	1428	K_6C_{60}
Rb	1447	Rb_3C_{60}
	1429	Rb_6C_{60}
Cs	1429	Cs_6C_{60}

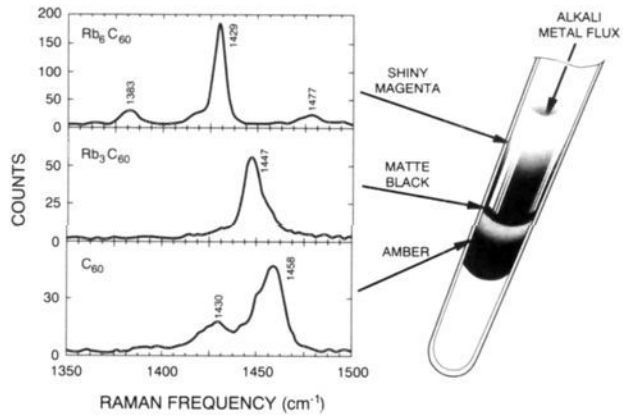

Figure 1. Raman spectra of a Rb-doped C_{60} film at room temperature.

Results

Raman Spectroscopy. Previous work has shown the A_g Raman mode to be sensitive to the state of C_{60} reduction.[3] Spectra of the doped films were probed along the length of the films, and results are summarized in Table I. Typical spectra for a Rb-doped film are shown schematically in Figure 1. The upper, most highly doped band shows a resolution-limited (7-cm^{-1} fwhm) mode at 1429 cm^{-1}. This has been identified with the Rb_6C_{60} phase. The central band reveals a broader mode (15-cm^{-1} fwhm) centered near 1447 cm^{-1}, identified as the Rb_3C_{60} phase. This change occurs abruptly at the visible interface between these bands, and we could find no evidence for any intermediate doping level. The spectrum of the lowest band is identical to an undoped film and is extremely sensitive to oxygen exposure of the C_{60} film prior to doping.[25] When precautions are taken to exclude oxygen, only a broad, 1458-cm^{-1} mode is found; otherwise, a sharp 1467-cm^{-1} mode is superimposed.[25] We can assert that no features are seen in Raman spectra of the lowest band which are not seen in undoped films, but because of the breadth of the modes, the possibility of solid solutions with variable levels of doping can not be excluded.

Raman spectra for K- and Rb-doped films were identical in all respects. With Cs-doped films, however, only a single interface was visible and Raman spectra changed abruptly from the undoped spectrum to the 1429-cm^{-1} mode for Cs_6C_{60} at this interface. There was no visible or Raman indication of a less highly doped state. Na-doped films showed bands similar to those in the K- and Rb-doped films, but some differences were observed in the Raman spectroscopy. The central band mode frequency was 1449 cm^{-1}, slightly higher than observed in the K- and Rb-doped films. The most heavily doped band showed this mode at 1433 cm^{-1}, 5 cm^{-1} higher than observed in the K- and Rb-doped films. While these reduced shifts may result from variations in stoichiometry or incomplete charge transfer, further work, including X-ray diffraction, is required for a clearer understanding of the Na-doped films. A detailed analysis of Raman spectra of the doped films will be published separately.[26]

(22) Glarum, S. H.; Marshall, J. H.; Schneemeyer, L. F. *Phys. Rev.* **1988**, *37B*, 7491–7495.
(23) Glarum, S. H.; Schneemeyer, L. F.; Waszczak, J. V. *Phys. Rev.* **1990**, *41B*, 1837–1841.
(24) Haddon, R. C.; Glarum, S. H.; Chichester, S. V.; Ramirez, A. P.; Zimmerman, N. M. *Phys. Rev.* **1991**, *43B*, 2642–2647.
(25) Duclos, S. J.; Haddon, R. C.; Glarum, S. H.; Hebard, A. F.; Lyons, K. B. *Solid State Commun.* **1991**, *80*, 481–484.

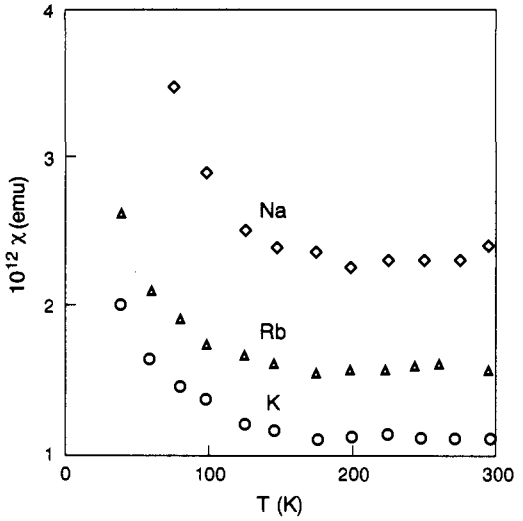

Figure 2. Paramagnetic susceptibilities for Na-, K-, and Rb-doped C_{60} films obtained from integrated ESR spectra. The values shown are for actual samples and are not normalized with respect to sample sizes (estimated to be of the order of 10^{-8} mol).

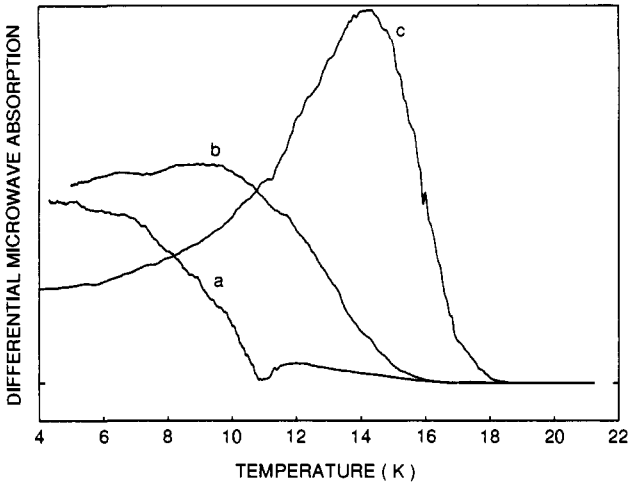

Figure 3. Evolution of superconductivity as seen by differential microwave loss in a 100-G field during K-doping of a C_{60} film: (a) initial response after 80 min of doping at 130 °C; (b) after 40 min of additional doping; (c) after 32 h of annealing at 220 °C. The magnitude of the modulated loss is shown versus temperature.

Electron Spin Resonance. One of the first indications of doping in C_{60} films is the appearance of an ESR absorption, $g = 1.9994$ (K), $g = 2.0000$ (Rb), which immediately precedes the appearance of superconductivity. For films showing the strongest superconducting response, we observed a maximum ESR signal with the central band centered in the cavity (±0.5 mm), $g = 1.9999$ (K), $g = 2.0005$ (Rb). For Na-doped films, which revealed no superconductivity above 4 K, $g = 2.0011$. The susceptibilities derived from integrated ESR spectra are plotted in Figure 2 as a function of temperature. Heavily overdoped films frequently showed new absorptions with g values greater than the free-spin values (2.0052 (Na), 2.0044 (K), 2.0028 (Rb), 2.0026 (Cs)).

Microwave Loss—Superconductivity. Microwave loss measurements presently offer the most sensitive technique for detecting superconductivity. In our experiments, the sample sits in a microwave magnetic field ~20 mG. Viewing the superconducting band as a hollow cylinder, this field lies parallel to the cylinder's axis. A static magnetic field is applied perpendicular to this axis, and a modulation field, parallel to the static field, is superimposed. Our typical experiment for characterization is to use a 100-G static field and a 3-G_{rms}, 100-KHz modulation field. The magnitude

(26) Duclos, S. J.; Haddon, R. C.; Glarum, S. H.; Hebard, A. F.; Lyons, K. B. *Science* **1991**, *254*, 1625–1627.

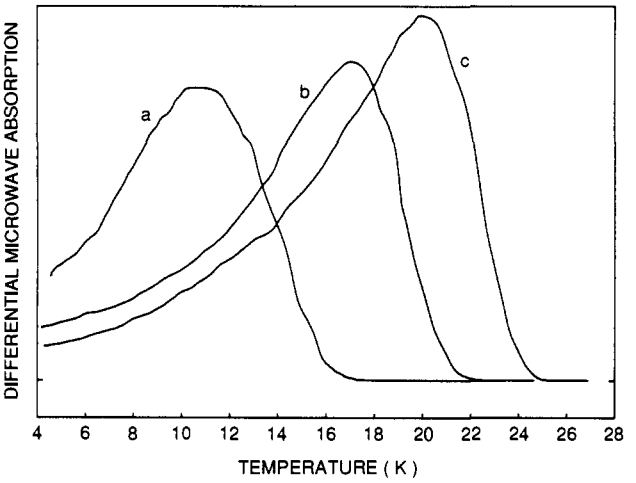

Figure 4. Evolution of superconductivity as seen by differential microwave loss in a 100-G field during Rb-doping of a C_{60} film: (a) initial response after 5 h of doping at 100 °C; (b) after 30 min of annealing at 120 °C; (c) after 3 h annealing at 120 °C.

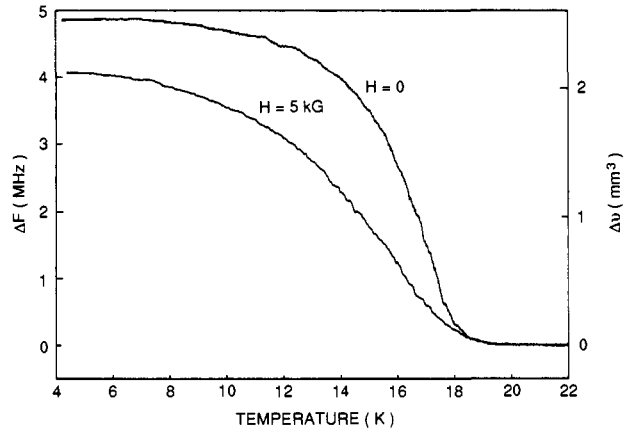

Figure 5. Variation of the microwave cavity resonance frequency with temperature for a K-doped C_{60} film. No modulation fields were applied. The right-hand ordinate indicates the equivalent spherical flux exclusion volume (1.93 MHz/mm³).

of modulated microwave loss is then measured as the temperature is lowered, the usual scan taking 10 min. In the absence of superconductivity, there is no background field-dependent loss and the detector can run at maximum sensitivity. The signals for the K and Rb films were 50000 times greater than the inherent noise level, even though loss only occurs within a superconducting region of but a few micrograms. Within this limit, no indications of superconductivity were found in Na- or Cs-doped C_{60} films, or in C_{70} films doped with Na, K, Rb, or Cs.

Figure 3 shows several stages in the evolution of a K-doped superconducting film. In the early stages, the principal rise in the signal occurs well below T_c, although there is a weak tail extending up to 16–17 K. The apparent node near 11 K is an artifact in measuring the magnitude of modulated loss. Above this node, the phase angle of modulated loss is 180°, below it, 0°; i.e., loss is decreasing with the field at higher temperatures and increasing with the field at lower temperatures. We also noted a marked rise in the dc bias of the microwave crystal detector just below T_c. This is a direct sign of increasing cavity loss which is independent of modulation fields.

On continued doping, the 180° phase region narrows to a fraction of a degree below T_c, although the response still appears depressed immediately below T_c. Annealing was tried when the signal was no longer significantly improved by doping. Optimal temperatures appeared to be around 200 °C as a slight decrease in response was found at 250 °C (K-doped films). Annealing increases the signal amplitude, eliminates the 180° onset phase angle, and shifts the maximum toward higher temperatures, as

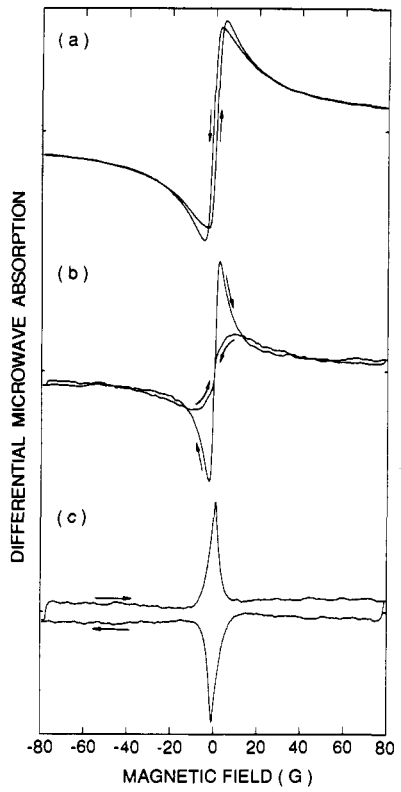

Figure 6. Field dependence of modulated microwave loss for a Rb-doped C_{60} film at 20 K during continuous field cycling. Peak to peak modulation fields are (a) 5 G, (b) 0.5 G, and (c) 0.05 G.

well as increasing T_c (Figure 3). Qualitatively, the response of films to K- and Rb-doping is much the same (Figure 4). The main difference is that for K-doped films T_c increased from 17 to 19 K upon annealing, whereas with Rb-doped films it could be raised to 25 K. This latter value is still below the values of 28–30 K found for doped powders.[5,6]

Microwave Flux Exclusion. One unusual property of these superconducting films was the large increase in the resonant frequency of the microwave cavity below T_c (Figure 5). As shown by Maier and Slater,[27] this frequency shift comes from the exclusion of the microwave magnetic field from a sample and is directly proportional to an exclusion volume. A calibration of our cavity with steel spheres gave 1.93 MHz/mm^3. The observed shifts correspond to equivalent spherical volumes greater than 2 mm^3, over 1000 times the true sample volume and apparently reflective of the film's 1-mm radius.

Field-Dependent Microwave Loss. Figure 6 shows the variation in modulated microwave loss for a Rb-doped film as a function of a slowly varying magnetic field. The distinctive changes at $H = 0$ are very familiar from studies of high-T_c materials and are associated with weak links in polycrystalline superconductors.[22] For large-amplitude modulation fields, curve a, behavior is reversible and the signal amplitude proportional to the modulation amplitude, until distorted by modulation broadening. The shape of curve a is the derivative of a microwave absorption minimum at $H = 0$, and extrema at ±3 G (corrected for broadening) measure the width of this minimum. For very small modulation fields, curve c, response is totally hysteretic and also increases with the modulation field's amplitude. In the transition region, centered about a 0.1-G_{pp} modulation amplitude, the shapes are complex, curve b, and the peak to peak signal amplitude varies little with modulation.

Discussion

ESR Spectra. Above 150 K, the susceptibility is temperature-independent, suggesting Pauli paramagnetism characteristic of conduction electrons (Figure 2). A rough estimate of the sample volume, assuming a band 1 mm wide and 0.5 μm thick, yields a Fermi level density of 2 levels/eV per C_{60}. Within the uncertainties of effective volumes, the magnitudes are similar for Na-, K-, and Rb-doped films. Below 150 K, the ESR spectrum is dominated by $1/T$ Curie behavior, corresponding to 1 spin/100 C_{60} molecules, assuming the same effective volume. No measurable g value difference was noted for the Curie and Pauli contributions.

This Fermi level density of states is in good agreement with recent photoemission measurements.[17] EHT band structure calculations give 6.5 levels/eV per C_{60},[28] while NMR measurements[16] of the ^{13}C spin–lattice relaxation time give a value of 20 levels/eV per C_{60}. The narrow bandwidth found in critical field measurements is also consistent with a high density of states.[21] The origin of the discrepancies in the density of states estimates remains to be resolved.

At 300 K, the major contribution to the Pauli susceptibility for all three dopants comes from a resonance 6 G wide with g values of 2.000–2.001. Superimposed is a narrower resonance, 1 G wide, with virtually the same g value. The Curie contribution, which dominates the low-temperature susceptibility, stems from this sharper resonance. The insensitivity of the conduction electron spin resonance linewidth to the alkali metal indicates that the electronic wave functions do not have a significant alkali-metal component. For the pure metals, we can only see an ESR signal with Na and K. At 50 K the linewidths for thin films of Na and K are 2.5 and 32 G, respectively, with g values of 2.0011 and 1.9968. Larger spin–orbit interactions with Rb and Cs shorten the spin state lifetimes, and the absorptions are too broad to be detected.

A g value less than the free-spin value, 2.0023, is characteristic of C_{60} negative ions, Allemand and co-workers[29] report 1.9991 for a tetraphenylphosphonium salt of C_{60}^-. This value is close to those we find for the nominally trinegative anion in A_3C_{60}, suggesting that the C_{60} molecular orbital coefficients and energies have not been greatly affected by the increased charge. It has been proposed that this g value, which is anomalously low for an aromatic hydrocarbon, results from the 3-fold LUMO orbital degeneracy. However, a quantitative explanation is still lacking, and the significance of the smaller cation-dependent variations in these films are not clear. The source of the Curie paramagnetism has not been identified, although it seems reasonable, because of its g value, to associate it with C_{60} defect centers. Under no doping conditions have we found a Curie spin density of stoichiometric magnitude, as in the phosphonium salts.

Microwave Flux Exclusion. Flux exclusion comes from microwave currents circulating around the superconducting band and is quenched by imperfections interrupting this flow. The effect arises from the difference in microwave field penetration between the normal and superconducting states. A 500 S/cm conductivity has been reported for K-doped films.[3,10] The corresponding 9-GHz skin depth is 25 μm, much more than the film's thickness, so the film is transparent to microwave fields above T_c. When the sample goes superconducting, however, penetration is reduced to the London length (λ_L), and if this is less than the film's thickness, flux will be excluded from the interior of the superconducting band as well as the film itself. For a disk of radius a with a magnetic field parallel to its axis, Maier and Slater[27] calculate an exclusion volume of $16a^3/9$, close to that observed. (We are unaware of a calculation for the screening coefficient of a ring.)

Microwave flux exclusion sets the film thickness (estimated to be 0.5 μm in the vicinity of the superconducting band) as an upper limit for λ_L. This limit is consistent with the 0.24-μm value reported for powders[21] and with the value of 0.48 μm found for a pressed pellet by muon spin relaxation measurements.[30] We

(27) Maier Jr., L. C.; Slater, J. C. *J. Appl. Phys.* **1952**, *23*, 68–77.

(28) Haddon, R. C.; Hebard, A. F.; Rosseinsky, M. J.; Murphy, D. W.; Glarum, S. H.; Palstra, T. T. M.; Ramirez, A. P.; Duclos, S. J.; Fleming, R. M.; Siegrist, T.; Tycko, R. Carbon Clusters. *ACS Symp. Ser.* **1992**, *481*, 71–89.

(29) Allemand, P.-M.; Srdanov, G.; Koch, A.; Khemani, K.; Wudl, F.; Rubin, Y.; Diederich, F.; Alvarez, M. M.; Anz, S. J.; Whetten, R. L. *J. Am. Chem. Soc.* **1991**, *113*, 2780–2781.

also note that the magnitude of the frequency shift responds to annealing, a larger volume exclusion correlating with a higher maximum in plots such as Figures 3 and 4. The maximum flux exclusion values observed were similar for K- and Rb-doped films.

Figure 5 also reveals that, in a 5000-G field, the excluded volume is reduced only 16%. At 9 GHz, a conductivity greater than 10^6 S/cm is required for flux exclusion by a 1-μm film. The Bardeen–Stephen equation, $\sigma(H) = \sigma_0 H_{c2}/H$, with σ_0 the normal state conductivity and H_{c2} the upper critical field, connects field and resistivity in type II superconductors. The value $\sigma_0 = 500$ S/cm implies $H_{c2} > 10^7$ G.

The long-lived spin states shown by conduction ESR indicate that paramagnetic pair breaking will lead to a first-order transition at the Clogston[31,32] limit when the spin level splitting equals the superconducting gap energy, $g\beta H = \Delta_0/\sqrt{2}$, as noted by Holczer and co-workers.[21] Our H_{c2} estimate, based on a linear extrapolation of low-field loss, is significantly higher than that found from $T_c(H)$ measurements and consistent with the view that the latter is set by paramagnetic pair breaking.[33,34]

Microwave Loss—Superconductivity. The shapes of the plots of differential loss vs temperature in Figures 3 and 4 are also typical of polycrystalline $YBa_2Cu_3O_7$ materials in which weak links provide the dominant loss mechanism.[35] Single crystals, in contrast, show a very abrupt rise at T_c to a maximum within a fraction of a degree and a rapid drop to the base line a few degrees below T_c.[23,24]

The 180° phase angle seen near T_c is anomalous, and we suggest that this is due to the nonuniform current distribution surrounding isolated superconducting patchs. When such a patch goes superconducting, its contribution to the observed loss decreases but it also "attracts" currents toward it, increasing the current density in the enveloping resistive region. The net result is an increase in total loss (Appendix I). As only loss in the superconducting patch is field-dependent, the apparent phase of the modulated loss is reversed. This situation requires that the fields of separate patches do not significantly overlap; i.e., the separation of patches must exceed their dimensions. As patch density increases or the intervening material turns superconducting, the current distribution will tend toward uniformity and a "mean" behavior.

The low-field behavior shown in Figure 6 is also a well-documented characteristic of weak links.[23,36,37] Although often discussed, there is still no generally accepted interpretation in terms of conventional weak-link parameters. From the flux quantization relation, $HA = \Phi_0$, an area A of 7 μm^2 may be inferred from the 3-G extrema which measures the width of the reversible loss minimum at $H = 0$. This area has been interpreted in terms of either a grain or junction size.[35,38] In the latter case, the junction width is $\sim 2\lambda_L$ and the effective junction length either a physical length or a Josephson penetration distance, λ_J.[39,40]

The basic dissipation mechanism involves the displacement of flux in weak links by microwave currents flowing across junctions.[41] Flux motion modulates the phase difference across the junction, a voltage is thereby induced, and a resistive current is set up across the junction with an ensuing V^2/R dissipation, R being the junction's normal resistance. In low magnetic fields, a theoretical junction resists flux penetration up to a critical field; $H_c = \Phi_0/(2\pi\lambda_L\lambda_J)$.[42] Taking $H_c = 3$ G and $\lambda_L = 0.25$ μm, we obtain $\lambda_J = 4$ μm or a maximum junction tunneling current density, $J_0 = 3 \times 10^3$ A/cm^2. At low modulation amplitudes the response becomes fully hysteretic, with the crossover centered about a peak to peak modulation amplitude of 0.1 G. The origin of this hysteresis is unresolved. It may reflect a trapping of vortices within weak links by a spatially varying J_0, with barriers inhibiting the annihilation of vortices and antivortices. For a barrier of width λ_L, the 0.1-G amplitude implies a barrier current density, $J = cH/4\pi\lambda_L$, also 3×10^3 A/cm^2. The 180° phase reversal of modulated loss with sweep direction is then rationalized in terms of a modulation of a vortex density in one direction and an antivortex density in the reverse, with barriers frustrating their equilibration. In a model proposed by Dulcic et al., the reversible curves are attributed to a tunneling diffraction profile; i.e., their width is inversely proportional to a junction length, and the hysteresis to critical state shielding currents.[40] This model leads to a reversible curve which is approximately the derivative of the hysteretic curve. However, in Figure 5, curve c is narrower than curve a and, in this regard, these films differ from typical polycrystalline $YBa_2Cu_3O_7$ results.

The magnetic fields characterizing low-field microwave loss are remarkably similar for doped-C_{60} films and polycrystalline $YBa_2Cu_3O_7$ materials, suggesting that, whatever the appropriate interpretation, the underlying parameters are rather similar. What seems more surprising is the strong influence of weak links in the films. The $YBa_2Cu_3O_7$ materials are highly anisotropic, and the weak links are usually attributed to mismatched grain boundaries. The K_3C_{60} structure, on the other hand, is cubic, and it is not obvious why the boundaries in polycrystalline films should be so effective in flux trapping at low fields.

The magnitudes of the microwave loss signals in these thin films are considerably greater than those we have seen in other superconductors. Responses from comparable $YBa_2Cu_3O_7$ films are less by a factor of 100, although showing behaviors similar to those in Figures 3 and 4. All other factors being equal, we expect dissipation to scale with the normal state resistivity. This difference is consistent with the reported values of 2×10^{-3} Ω cm for K_3C_{60}[3,10] and 10^{-4} Ω cm for $YBa_2Cu_3O_7$.[43] When similar amounts of powdered samples of these materials are compared, however, signals from the latter are 100 times greater. Whether this difference is due to differing conductivities or the absence of superconducting intergranular contacts in A_3C_{60} powders has not been resolved.

Thermal annealing also plays an important part in improving the superconducting characteristics of thin films. This may be due to a more uniform distribution of dopant or the growth of better ordered regions. Possibly the weak links result from the segregation of impurities in intergranular boundaries during grain growth. T_c increases on annealing, especially in the case of Rb. Given the short coherence length implicit in a high H_{c2}, T_c will reflect short-range structural order and its increase indicates some compositional variability. While the presence of discrete phases rules out continuous compositional variations, there remains a finite range of variability within the superconducting phase.

Finally, we take note of doping kinetics. It is evident visually that doping proceeds heterogeneously, with well-defined interfaces separating the superconducting phase from overdoped and underdoped regions. If doping were limited by metal diffusion within the film, we should expect to find lateral rather than longitudinal inhomogeneities (Figure 1). An effusional calculation for 10^{-4} Torr and 100 °C indicates that about 10 min is required to dope

(30) Uemura, Y. J.; Keren, A.; Le, L. P.; Luke, G. M.; Sternlieb, B. J.; Wu, W. D.; Brewer, J. H.; Whetten, R. L.; Huang, S. M.; Lin, S.; Kaner, R. B.; Diederich, F.; Donovan, S.; Gruner, G.; Holczer, K. *Nature* **1991**, *352*, 605–607.
(31) Clogston, A. M. *Phys. Rev. Lett.* **1962**, *9*, 266–267.
(32) Chandrasekhar, B. S. *Appl. Phys. Lett.* **1962**, *1*, 7–8.
(33) Hackett Jr., W. H.; Maxwell, E.; Kim, Y. B. *Phys. Lett.* **1967**, *24A*, 663–664.
(34) Kim, Y. B.; Stephens, M. J. In *Superconductivity*; Parks, R. D., Ed.; Marcel Dekker: New York, 1969; p 1107.
(35) Bohandy, J.; Kim, B. F.; Adrian, F. J.; Moorjani, K. *Phys. Rev.* **1989**, *39B*, 2733–2735.
(36) Khachaturyan, K.; Weber, E. R.; Tejedor, P.; Stacy, A. M.; Purtis, A. M. *Phys. Rev.* **1987**, *B36*, 8309–8314.
(37) Blazey, K. W.; Muller, K. A.; Bednorz, J. G.; Berlinger, W.; Amoretti, G.; Buluggiu, E.; Vera, A.; Mattacotta, F. C. *Phys. Rev.* **1987**, *B36*, 7241–7243.
(38) Peric, M.; Ravkin, B.; Prester, M.; Brnicevic, N.; Dulcic, A. *Phys. Rev.* **1988**, *B37*, 522–524.
(39) Blazey, K. W.; Portis, A. M.; Bednorz, J. G. *Solid State Commun.* **1988**, *65*, 1153–1156.
(40) Dulcic, A.; Ravkin, B.; Pozek, M. *Europhys. Lett.* **1991**, *10*, 593–598.
(41) Portis, A. M.; Blazey, K. W. *Solid State Commun.* **1988**, *68*, 1097–1100.
(42) Tinkham, M. J. *Introduction to Superconductivity*; McGraw-Hill: New York, 1975; p 201.
(43) Cava, R. J.; Batlogg, B.; van Dover, R. B.; Murphy, D. W.; Sunshine, S.; Siegrist, T.; Remeika, J. P.; Rietman, E. A.; Zahurak, S. M.; Espinosa, G. P. *Phys. Rev. Lett.* **1987**, *58*, 1679.

100 μg of C_{60} to the K_6 level when vapor transport is rate limiting. The observed rate is significantly slower, suggesting that additional factors such as nucleation and adsorption kinetics may be important. A relevant question is whether doping is reversible and chemical equilibria exists at the vapor–C_{60} interface. We have not succeeded in undoping any films to date by localized heating. At temperatures of 400–500 °C, we see only the growth of an ESR absorption with a g value greater than free spin and we attribute this to decomposition products. With these thin films it therefore appears that the doping process is not reversible with respect to interphase conversion but determined by kinetics. Our ability to form well-defined superconducting regions is a fortuitous happenstance of macroscopic phase boundaries able to adjust to increasing doping.

Conclusions

In our study of the doping of C_{60} films we have discovered that the films give rise to multiple phases which remain discrete as the dopant moves laterally along the film. We report the first observation of superconductivity in an Rb_3C_{60} film (T_c = 25 K). Potassium and rubidium dopants behave similarly. Both metals give rise to A_3C_{60} and A_6C_{60} phases, and the A_3C_{60} compositions are superconductors. Potassium-doped films readily attain the T_c of 19 K exhibited by the bulk materials, but this is not the case for rubidium doping. Sodium doping also produces the A_3C_{60} and A_6C_{60} phases, but superconductivity was not detected down to 4 K. Cesium only gave rise to the A_6C_{60} phase. None of these alkali metals gave rise to superconductivity with C_{70} films.

Acknowledgment. We are grateful to R. M. Fleming, A. F. Hebard, K. B. Lyons, B. Miller, D. W. Murphy, T. T. M. Palstra, K. Raghavachari, A. P. Ramirez, M. J. Rosseinsky, and R. Tycko for valuable contributions to this work.

Appendix

Consider a spherical region, radius a and conductivity σ_2, embedded concentrically in a much larger spherical region, radius R and conductivity σ_1. The electric field is given by potential theory

$$\vec{E} = -\vec{\nabla}V \qquad \nabla^2 V = 0 \tag{A1}$$

and the current density and dissipation are

$$\vec{J} = \sigma\vec{E} \qquad D = \int d\tau\, \sigma\vec{E}\cdot\vec{E} \tag{A2}$$

Formal solutions to Laplace's equation in three dimensions are

$$r > a \qquad V_1 = -E_0 r\cos\theta + (B/r^2)\cos\theta \tag{A3}$$

$$r < a \qquad V_2 = Cr\cos\theta$$

with E_0 the field far from the origin and B and C coefficients to be found from the boundary conditions at $r = a$.

$$V_1(a) = V_2(a) \tag{A4}$$

$$\sigma_1 \partial V_1/\partial r = \sigma_2 \partial V_2/\partial r$$

Upon solving for B and C, the field may be evaluated. For a current-driven system, $J_0 = \sigma_1 E_0$ and the combined dissipation in regions 1 and 2 is found to be

$$D = (4\pi R^3/3\sigma_1)J_0^2 + (4\pi a^3/3\sigma_1)[(\sigma_2 - \sigma_1)/(2\sigma_1 + \sigma_2)]J_0^2 \tag{A5}$$

When the core region goes superconducting, $\sigma_2 > \sigma_1$ and total dissipation increases. Although core dissipation vanishes in the limit $\sigma_2 \to \infty$, this reduction is more than compensated by the increased current density in the surrounding shell. We now assume that only the resistivity of the core region, $\rho_2 = 1/\sigma_2$, is magnetic field dependent. According to the Bardeen–Stephen approximation $\rho \propto H$, but in general we expect $\partial\rho_2/\partial H > 0$. Thus, the field dependence of dissipation becomes

$$\partial D/\partial H = -4\pi a^3 J_0^2(\partial\rho_2/\partial H)[\sigma_2/(2\sigma_1 + \sigma_2)]^2 \tag{A6}$$

and we find that loss always decreases with increasing field. A current density J_0 in the core would give a dissipation

$$D_0 = (4\pi a^3/3)J_0^2/\sigma_2 \tag{A7}$$

and consequently

$$\partial D/\partial H = -3(\partial D_0/\partial H)[\sigma_2/(2\sigma_1 + \sigma_2)]^2 \tag{A8}$$

The phase of the modulated loss response is reversed, and in the limit $\sigma_2 \gg \sigma_1$, its magnitude is enhanced 3-fold over that for a uniform current distribution.

In two dimensions with cylindrical symmetry, an analogous calculation yields

$$\partial D/\partial H = -4(\partial D_0/\partial H)[\sigma_2^2(\sigma_2 - 3\sigma_1)/(\sigma_1 + \sigma_2)^3] \tag{A9}$$

For $\sigma_2 \gg \sigma_1$, the enhancement is −4 but phase reversal requires $\sigma_2 > 3\sigma_1$.